ACS APPLIED MATERIALS & INTERFACES

Research Article

www.acsami.org

Reactive-Template Fabrication of Porous SnO_2 Nanotubes and Their Remarkable Gas-Sensing Performance

Jun Zhang,* Jing Guo, Hongyan Xu, and Bingqiang Cao*

Key Laboratory of Inorganic Functional Materials in Universities of Shandong, School of Materials Science and Engineering, University of Jinan, Jinan 250022, China

ABSTRACT: A facile reactive-template strategy has been developed to fabricate porous SnO_2 nanotubes using MnO_2 nanorods as the sacrificial template. The formation of nanotubes is based on the redox reaction mechanism, which requires no post-treatment of the MnO_2 templates. The morphological and structural characteristics of the samples have been systematically characterized by X-ray powder diffraction (XRD), scanning electron microscopy (SEM), transmission electron microscopy (TEM), thermal-gravimetric (TG), and N_2 adsorption−desorption techniques. A gas-sensor device was constructed using as-prepared SnO_2 nanotubes and was tested for its ability to detect ethanol and some other compounds. Because of the porous structure and relative large specific surface area, the SnO_2 nanotube sensor manifests remarkably improved sensing performance, including fast response recovery, high sensitivity, and excellent repeatability, suggesting the promising application of the SnO_2 nanotube materials.

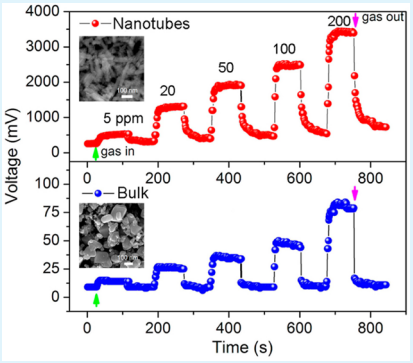

KEYWORDS: *SnO_2, nanotubes, porous, gas sensor, high performance*

1. INTRODUCTION

Nanostructured metal oxides with a hollow and/or porous structure have received considerable attention in many applications, including lithium-ion batteries,[1−3] supercapacitors,[4] solar cells,[5] photocatalysts,[6] and chemical gas sensors,[7,8] resulting from their unique structural features. In particular, the 1D tubular structures of metal oxides are even more appealing because of their robust structure, large surface-to-volume ratio, improved surface area, and easily accessible inner surface to guest molecules. These properties make them highly promising for use in functional devices with high performance. For example, SnO_2 nanotubes have demonstrated enhanced electrochemical properties in lithium-ion battery applications.[9−11] SnO_2 nanotubes have been prepared using anodic aluminum oxide (AAO) membranes,[11] silica nanorods,[9] MoO_3 nanorods,[12] carbon nanotubes,[13] and cellulose fibers[14] as the template. It has been stated that the hollow structure of SnO_2 nanotubes could greatly facilitate electron transportation, increase electrode contact with the electrolyte, and alleviate electrode volume change in charge/discharge processes.

Another prominent example is the utilization of metal-oxide nanotubes for use in high-performance gas-sensing devices.[14−17] Chen et al.[16] have reported the enhanced sensing properties of α-Fe_2O_3 nanotubes prepared using AAO as the template. Song and co-workers[15] have shown that the porous NiO nanotubes derived from the controlled oxidation of preformed Ni_3S_2/Ni core−shell nanorods possess improved gas-sensing performance toward ethanol. It is noted that the aforementioned metal-oxide nanotubes are mainly fabricated using the template method, where the template matrix is first conformally coated or filled with the desired metal-oxide precursors. In a subsequent step, the template is removed via thermal calcination or chemical etching to generate the tubelike nanomaterials. The template strategy is versatile, fabricating various structured nanotubes such as straight and helical tubes depending on the morphology of the template.[9] However, the template procedure usually suffers from tedious and multiple-synthesis processes; hence, it is time consuming. Furthermore, it might also pose a risk to contaminating the final product resulting from the incomplete removal of the template. Hence, it is of great interest to develop a facile protocol for fabricating nanotube materials by a template-free method or a reactive-template process that requires no post-treatment of the template. Pioneering works[18−22] have shown that ZnO micro/nanotubes can be obtained by a one-step solution process through the self-corrosion of ZnO micro/nanorods. Jia et al.[16,23] have also shown that α-Fe_2O_3 nanotubes can be formed by simply extending the hydrothermal reaction time in the presence of $NH_4H_2PO_4$ as the additive. α-Fe_2O_3 nanotubes have also been obtained by templating against ZnO nanorods.[24] However, the facile fabrication of SnO_2 nanotubes has been rarely reported.

In this work, we report an alternative synthesis of porous SnO_2 nanotubes via a reactive-template method using MnO_2 nanorods as the sacrificial template. This procedure is based on the redox chemistry between reductive Sn^{2+} and oxidative MnO_2 in an acidic environment. In our previous publication,[25] we employed such a reactive-template method to synthesize

Received: May 24, 2013
Accepted: July 18, 2013
Published: July 23, 2013

   dx.doi.org/10.1021/am4019884 | ACS Appl. Mater. Interfaces 2013, 5, 7893−7898

conducting polymer polypyrrole nanotubes as well as its advanced nanocomposites with noble metals. The present work proves further the validity and universality of the reactive-template process for generating inorganic nanotubes. To gain some perspective on their potential application, as-synthesized SnO_2 nanotubes were used to fabricate a chemical gas-sensing device that exhibits superior performance in terms of fast response recovery, high sensitivity, and excellent repeatability when compared to bulk SnO_2 materials.

2. EXPERIMENTAL SECTION

2.1. Synthesis of MnO_2 Nanorods. The synthesis of MnO_2 nanorods followed that from our previous work.[25] Typically, 0.63 g of $KMnO_4$ and 0.25 g of $MnSO_4{\cdot}H_2O$ were dissolved in 40 mL of distilled water under stirring to form a homogeneous solution. The stock solution was then transferred into a Teflon-lined stainless steel autoclave (50 mL) and heated at 160 °C for 12 h. After reacting, the dark-brown precipitate was harvested by centrifugation, washed with water and ethanol, and dried at 80 °C.

2.2. Synthesis of SnO_2 Nanotubes. In a typical synthesis, 0.1 g of MnO_2 nanorods were dispersed in 35 mL of distilled water under sonication. Next, 0.3 mL of concentrated HCL was added into the mixture followed by the addition of 0.3 g of $SnCl_2{\cdot}2H_2O$. The mixture was stirred for ca. 20 min, transferred into a Teflon-lined stainless steel autoclave (50 mL), and heated at 120 °C for 4 h. The product was centrifuged, washed with water and ethanol, and dried at 60 °C. Finally, porous SnO_2 nanotubes were obtained by annealing the product at 500 °C for 2 h.

2.3. Characterization and Gas-Sensing Test. The samples were characterized by means of powder X-ray diffraction (Bruker, D8 Advance, Cu Kα, λ = 1.5418 Å), scanning electron microscopy (SEM, Shimadzu SS-550 and Quanta 250 FEG), transmission electron microscopy (TEM, JEOL-1400, 100 kV), thermal-gravimetric analysis (TG, Mettler-Toledo TGA/DSC 1/1600HT, 5 °C/min, air), and N_2 adsorption−desorption (JW-BK122W). The gas-sensing properties of the as-prepared SnO_2 nanotubes were tested on a WS-60A gas-sensor measurement system (HanWei Electronics, China) at 300 °C with a relative humidity of 30%. The gas sensor is fabricated by coating a slurry of SnO_2 nanotubes and deionized water onto an alumina tube (length 4 mm, diameter 1 mm) positioned with two Au electrodes and four Pt wires on both ends. A Ni−Cr alloy foil in the alumina tube is employed as a heater. Atmospheric air is used as the reference and dilute gases. A calculated amount of test gas such as ethanol is introduced into the test chamber by a syringe. Two electric fans installed in the chamber are used to make the gas homogeneous. After completing a test, the chamber was removed for sensor recovery. The sensor sensitivity is defined as the ratio $S = Ra/Rg$, where Ra and Rg are the sensor resistance in air and in target gas, respectively.

3. RESULTS AND DISCUSSION

The overall synthesis procedure for SnO_2 nanotubes is illustrated in Figure 1, which consists of two steps. α-MnO_2 nanorods (JCPDS 44−0141) were first prepared using a hydrothermal reaction.[25,26] The MnO_2 nanorods were then employed as a reactive template to afford the conformal coating

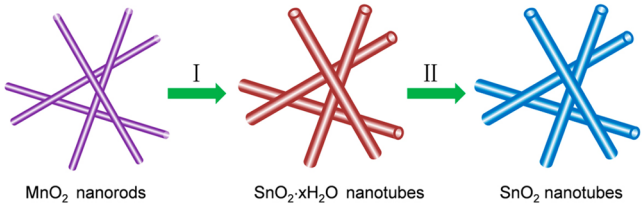

Figure 1. Syntheis process for SnO_2 nanotubes via a reactive-template strategy.

of $Sn(OH)_4$ or $SnO_2{\cdot}xH_2O$ using $SnCl_2$ as the Sn source via a hydrothermal process (step I). This process involves redox chemistry between MnO_2 and Sn^{2+}. It is known that the standard reduction potential of MnO_2/Mn^{2+} is ca. 1.22 V in acid media (eq 1), whereas that of Sn^{4+}/Sn^{2+} is 0.15 V, which is much lower than 1.22 V (eq 2). As a result, the MnO_2 nanorods could readily oxidize Sn^{2+} into Sn^{4+}. The Sn^{4+} released in this reaction would be confined to the vicinity of the MnO_2 nanowire surface to form a precipitation layer of hydroxide ($Sn(OH)_4$) because of the hydrolysis and comsumption of H^+ (eq 3). At the same time, the MnO_2 template is reduced to soluble Mn^{2+}. When the MnO_2 nanorods are completely dissolved because of reduction, then the $Sn(OH)_4$ nanotubes with a hollow interior are eventually formed. Under elevated temperature and autogenerated pressure (eq 4), the Sn hydroxide might transform into $SnO_2{\cdot}xH_2O$ with a rather poor crystallinity, as later proved by XRD analysis. TG anaysis in Figure 2 reveals that the sample

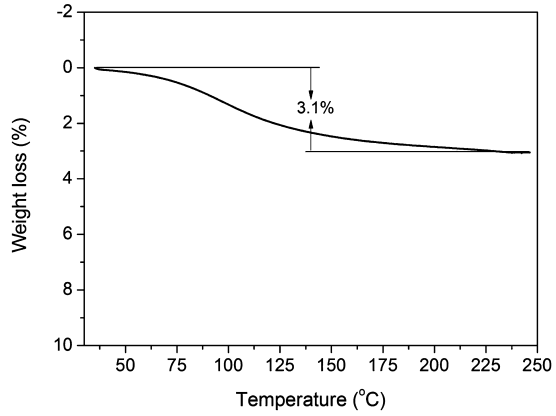

Figure 2. TG analysis of the sample before calcination.

exibits a total weright loss of only 3%, which can be ascribed to the evaporation of water moleclues in $SnO_2{\cdot}xH_2O$. In step II, the formed $SnO_2{\cdot}xH_2O$ nanotubes can be converted into pure SnO_2 by simply annealing (eq 5).

$$MnO_2 + 4H^+ + 2e \rightarrow Mn^{2+} + 2H_2O \quad (1)$$

$$Sn^{4+} + 2e \rightarrow Sn^{2+} \quad (2)$$

$$MnO_2 + Sn^{2+} + 2H_2O \rightarrow Mn^{2+} + Sn(OH)_4 \quad (3)$$

$$Sn(OH)_4 \rightarrow SnO_2{\cdot}xH_2O + (2 - x)H_2O \quad (4)$$

$$SnO_2{\cdot}xH_2O \rightarrow SnO_2 + 2H_2O \quad (5)$$

The crystallographic structure of the as-prepared nanotubes was examined by XRD, as shown in Figure 3. It reveals that the sample before calcination shows a very low diffraction intensity with pronounced peak broadening, indicating a poor crystallinity resulting from the low hydrothermal temperature. The nanotubes after calcination exhibit good crystallinity, and the diffraction peaks accord well with that of rutile SnO_2 (JCPDS 41-1445). The crystallite size of the SnO_2 nanotubes is estimated to be 11.3 nm using the Scherrer equation based on the full-width at half-maximum (fwhm) of the (110) diffraction peak. Furthermore, no obvious peaks for the MnO_2 nanorod template and other impurities can be detected in both patterns, suggesting that MnO_2 nanorods have been completely dissolved in the hydrothermal reaction. Figure 4a−c displays

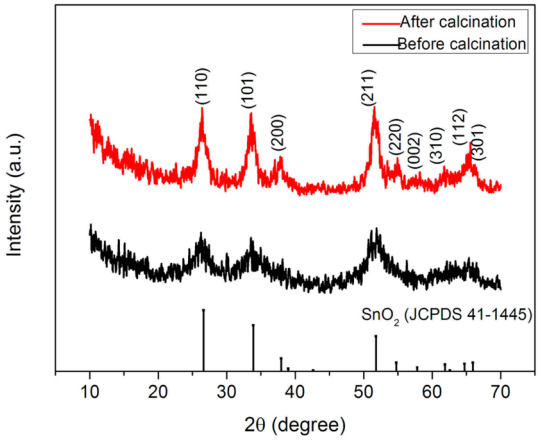

Figure 3. XRD patterns of the products before and after calcination.

the SEM images of the MnO_2 nanorods and the as-prepared SnO_2 nanotubes. The MnO_2 nanorods in Figure 4a have a 1D structure, with a longitude of several micrometers and diameter of tens of nanometers. The SnO_2 nanotubes in Figure 4b,c show a rough surface because the tube walls are composed of many nanoparticles. In addition, the SnO_2 nanotubes are observed to have a small length-to-diameter ratio compared to that of MnO_2 nanorods, which might be due to the rupture of MnO_2 nanorods caused by fast Sn^{2+} reduction in the hydrothermal process.

Further details of the as-prepared SnO_2 nanotubes can be seen in the TEM images in Figure 4d,e. In Figure 4d, the nanotubes are constituted by a large amount of nanoparticles with a size in the range of 5−15 nm. The hollow interior of the nanotubes are visible, as indicated by the dashed lines in Figure 4d,e. Furthermore, the nanotubes also manifest a porous structure because of the interparticle pores formed by the aggregation of the nanoparticles. The porous structure has been further confirmed by the N_2 adsorption−desorption isotherm in Figure 4f. The pore-size distribution (inset of Figure 4f) calculated using the Barrett−Joyner−Halenda (BJH) method for both the adsorption and desorption branches of the isotherm indicates that most of the pores have a diameter in the range of 2−6 nm. Such a porous structure leads to a Brunauer−Emmett−Teller (BET) specific surface area of 66.1 m^2/g.

Porous nanostructured materials have long been demonstrated to have great potential for many applications because of the advantages that arise from their unique structure. When used as sensing materials, the porous structure could enable a fast response recovery and high sensitivity resulting from enhanced gas diffusion and mass transportation as well as improved active surface area.[7,8,13,17,27,28] It is expected that as-prepared porous SnO_2 nanotubes would deliver a better sensing performance. Thus, a gas sensor was fabricated using the SnO_2 nanotubes as the active materials and preliminarily examined using ethanol and some other compounds as the target gases. For comparison, another gas sensor based on bulk SnO_2 particles was also fabricated and tested.

Figure 5a compares the dynamic response-recovery sensing curves of both gas sensors to different concentrations of ethanol (5, 20, 50, 100, and 200 ppm). It can be seen that both sensors exhibit a very fast response and recovery speed with gas in and out. The sensors also show very distinct responses to different ethanol concentrations. With increasing concentrations of

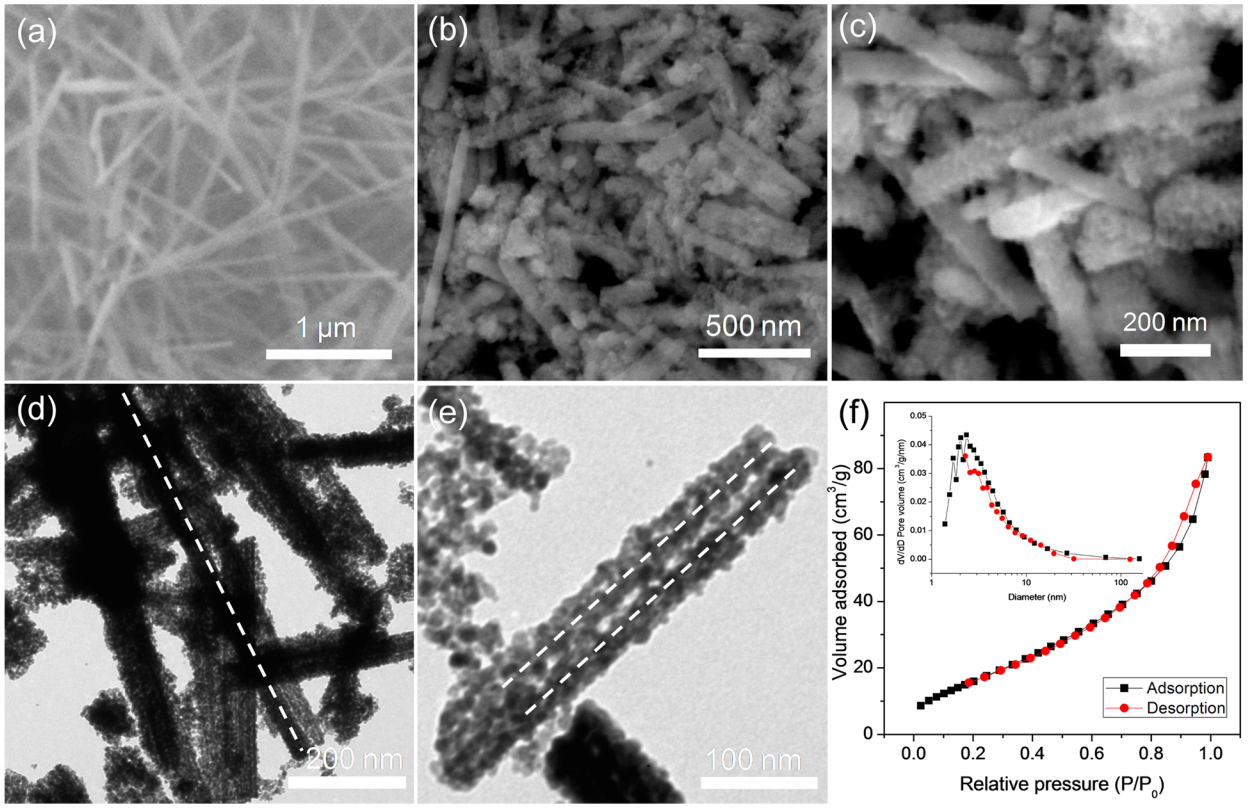

Figure 4. SEM images of (a) MnO_2 nanorods and (b, c) SnO_2 nanotubes. (d, e) TEM images of SnO_2 nanotubes. (f) N_2 adsorption−desorption isotherm with the BJH pore-size distribution in the inset.

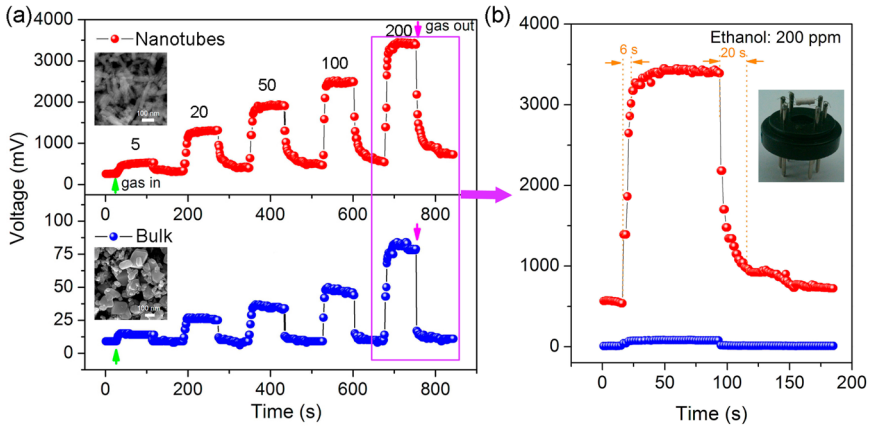

Figure 5. (a) Dynamic response-recovery sensing curves of SnO_2 nanotubes and bulk materials to different ethanol concentrations (5−200 ppm). (b) Comparison of the sensing performances to 200 ppm of ethanol (the inset is a photograph of the gas sensor device).

ethanol, the sensor sensitivity also shows a remarkable increase, indicating an excellent discrimination ability to varied gas concentrations. However, the SnO_2 nanotubes possess a much better response than that of the bulk SnO_2, which can be seen from the higher response amplitude to each ethanol concentration of the former sensor in comparison to that of the latter. For comparison, the sensing curves of both sensors to 200 ppm of ethanol are presented in Figure 5b. Obviously, the nanotube sensor shows a significantly higher signal, whereas that of the bulk SnO_2 sensor is almost negligible. The response-recovery curve of the SnO_2 nanotube sensor in Figure 5b also indicates a very short response time of 7 s and a quick recovery within 20 s. Their sensor sensitivities to different ethanol concentrations are compared in Figure 6, which suggests that

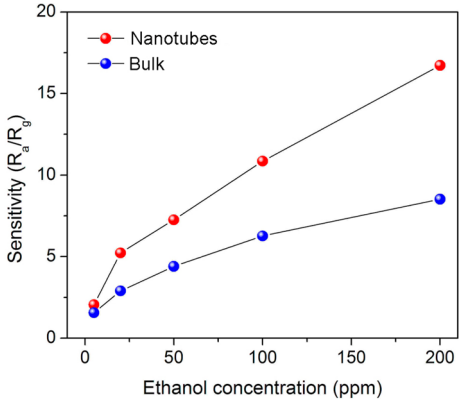

Figure 6. Sensor sensitivities of SnO_2 nanotubes and bulk materials to various enthanol concentrations.

the nanotubes are more sensitive than bulk SnO_2. To 200 ppm ethanol, the nanotube sensor has a sensitivity of 16.7, which is nearly two times higher than that (8.5) of bulk SnO_2. The superior sensor response of SnO_2 nanotubes over bulk SnO_2 particles probably results from the porous structure and large specific surface area of 66.1 m^2/g, which is nearly four times higher than that (17.5 m^2/g) of bulk SnO_2 particles. Furthermore, compared with previous works,[29,30] the gas sensors based on SnO_2 nanoparticles have been reported to show a response time longer than 20 s to 100 ppm ethanol, whereas the SnO_2 nanotube in this work has a response time of only several seconds (<6 s), as evaluated from Figure 5a. This further confirms the advantages of the SnO_2 nanotube structure in fabricating high-performance gas sensors.

The sensor sensitivity of SnO_2 nanotubes to several other compounds (all of the concentrations are 20 ppm) is also studied. The results shown in Figure 7a confirm that the nanotubes sensor has a higher sensitivity to all of the test gases than the bulk SnO_2. As show in Figure 7a, the SnO_2 nanotube sensor displays the highest sensitivity, with a value of up to 17.2 for glycol and 14.6 for butanol, which are much larger than that for ethanol (5.8), acetone (2.4), and methanol (1.9). It seems that the sensor is more sensitive to higher alcohols. The glycol molecule has two hydroxyls, which could exhibit stronger reducibility than ethanol, leading to a higher response in surface-sensing reactions with the chemisorbed oxygen species (O_2^-, O^-, and O^{2-}) on the SnO_2 surface.[29−31] Except for glycol and acetone, it is noted the sensor sensitivity shows an overall increase with the carbon chain number of alcohols (i.e., in the sequence of methanol < ethanol < butanol). Such a phenomenon has also been previously reported by Yeh et al.[30] They found that the hydrothermally prepared SnO_2 nanoparticles possessed a higher sensitivity to alcohols with a longer carbon chain,[30] although the reason to this finding remains unclear. This result is possibly related to the different chemical reactivity of the alcohols following different sensing mechanisms. In the sensing process, the alcohols will be oxidized by the oxygen species and decomposed into aldehydes or alkenes through two possible mechanisms of dehydrogenation or dehydration.[32] Another possibility might be related to the conversion of CH_2 groups into CO_2 and H_2O. The different carbon chains might pose a different effect on the sensing reactions.

Humidity is an important factor that might affect the gas-sensing properties of a semiconductor metal oxide.[33,34] The SnO_2 nanotube sensor has been thus investigated for detecting 100 ppm of ethanol under different relative humidities. As shown in Figure 7b, the relative humidity demonstrates a large influence on sensing performance. Overall, the sensor response amplitude manifests a decrease with the increase of relative humidity from 17 to 54%, and the response time of the sensor shows a significant extension from 3 to 11s. However, the influence of the relative humidity on the recovery process of gas sensors is not very significant. The adverse effect of high humidity on gas-sensor performance can be ascribed to the immeasurable chemisorption/physisorption of water molecules on the SnO_2 surface,[34,35] which might interfere with the sensing

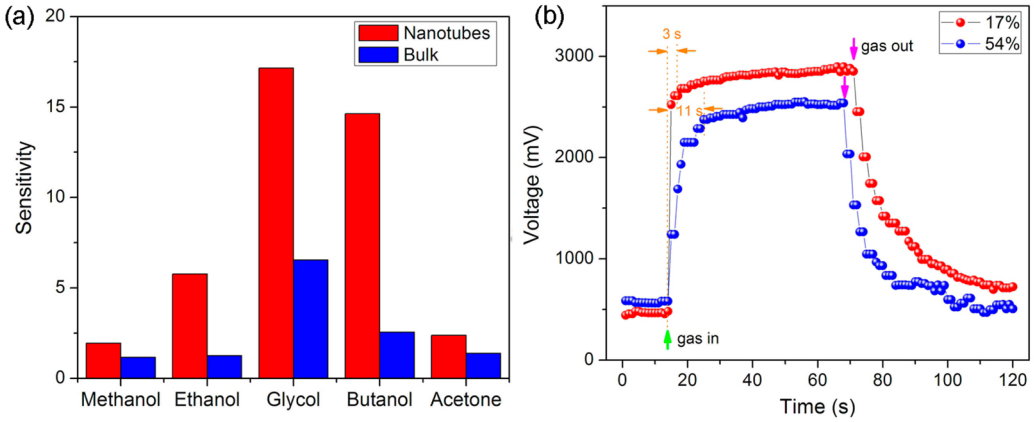

Figure 7. (a) Sensor sensitivities of SnO_2 nanotubes and bulk materials to various compounds (20 ppm). (b) Dynamic response-recovery sensing curves of SnO_2 nanotubes to 100 ppm of ethanol at different relative humidities (17 and 54%).

reactions by replacing the oxygen species preadsorbed on the SnO_2 surface, decreasing the activity of the sensing layer and retarding the response speed of gas sensors.

From the viewpoint of practical applications, gas sensors are expected to have good repeatability and stability. These parameters have been investigated by applying the SnO_2 nanotube sensor to successive gas-sensing tests in six cycles over a period of 4 months. As shown in Figure 8, the SnO_2 nanotube sensor exhibits a very fast response and recovery on successive gas-sensing tests in response to 100 ppm of ethanol, revealing an excellent repeatability even after 4 months. However, the long-term stability of the sensor is not very satisfactory. As can be seen, after working for 4 months the response of the sensor shows a decrease from its initial response amplitudes; however, it still features a very fast response-recovery characteristic. The decreased sensor stability may be caused by the structural change of the SnO_2 nanotubes over a long working time. Further effort is needed to improve the sensor stability for acquiring a long sensor life. Potentially, the decreased sensor performance might be alleviated by surface functionalization of the SnO_2 nanotubes with catalyst nanoparticles.

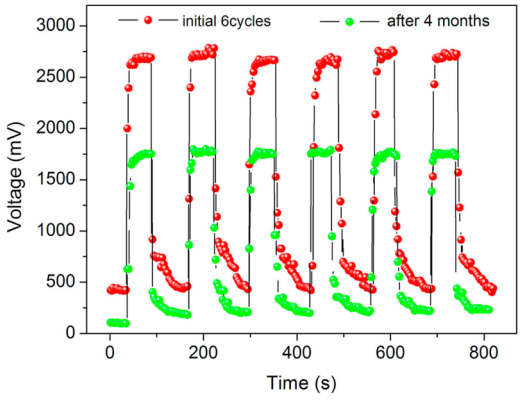

Figure 8. Repeatability and long-term stability of the SnO_2 nanotubes sensor (100 ppm of ethanol).

4. CONCLUSIONS

A reactive-template method using MnO_2 nanorods has been developed for fabricating SnO_2 nanotubes. This procedure requires no post-treatment or removal of the template. The reactive MnO2 nanorods serve as an oxidative platform to afford a conformal coverage of the Sn component. MnO_2 nanorods dissolved into the form of soluble Mn^{2+} on reduction by Sn^{2+}, and they simultaneously generated SnO_2 nanotubes with a hollow interior. Inspired by the unique porous structure, the SnO_2 nanotubes have been employed as the active materials to fabricate gas-sensing devices, which demonstrated excellent performance in terms of sensor sensitivity, fast response recovery, and repeatability, for alcohols. The SnO_2 nanotubes are also found to have much better sensor properties than bulk SnO_2 materials, which might result from their large specific surface area and hollow structures.

AUTHOR INFORMATION

Corresponding Author

*E-mail: mse_zhangj@ujn.edu.cn (J.Z.); mse_caobq@ujn.edu.cn (B.C.). Tel: 86-531-89736292.

Notes

The authors declare no competing financial interest.

ACKNOWLEDGMENTS

This work is supported by the program for New Century Excellent Talents in University (NCET-11-1027) from the Ministry of Education, China as well as the Shandong Provincial Science Foundation for Disguised Youth Scholars (JQ201214) and Excellent Young and Middle-aged Scientists (BS2012CL003). B.C. thanks the Taishan Scholar Professorship (TSHW20091007), and J.Z. thanks the Research Fund (XKY11111) for new faculty (both tenured at University of Jinan).

REFERENCES

(1) Wang, Z.; Zhou, L. *Adv. Mater.* **2012**, *24*, 1903−1911.
(2) Lou, X. W. D.; Archer, L. A.; Yang, Z. *Adv. Mater.* **2008**, *20*, 3987−4019.
(3) Cheng, F.; Tao, Z.; Liang, J.; Chen, J. *Chem. Mater.* **2007**, *20*, 667−681.
(4) Liu, J.; Jiang, J.; Bosman, M.; Fan, H. J. *J. Mater. Chem.* **2012**, *22*, 2419−2426.
(5) Zhu, K.; Neale, N. R.; Miedaner, A.; Frank, A. J. *Nano Lett.* **2007**, *7*, 69−74.
(6) Du, G.; Chen, Q.; Che, R.; Yuan, Z.; Peng, L.-M. *Appl. Phys. Lett.* **2001**, *79*, 3702−3704.
(7) Tiemann, M. *Chem.—Eur. J.* **2007**, *13*, 8376−8388.
(8) Lee, J.-H. *Sens. Actuators, B* **2009**, *140*, 319−336.

(9) Ye, J.; Zhang, H.; Yang, R.; Li, X.; Qi, L. *Small* **2010**, *6*, 296−306.
(10) Wang, Y.; Lee, J. Y.; Zeng, H. C. *Chem. Mater.* **2005**, *17*, 3899−3903.
(11) Wang, Y.; Zeng, H. C.; Lee, J. Y. *Adv. Mater.* **2006**, *18*, 645−649.
(12) Liu, B.; Zeng, H. C. *J. Phys. Chem. B* **2004**, *108*, 5867−5874.
(13) Jia, Y.; He, L.; Guo, Z.; Chen, X.; Meng, F.; Luo, T.; Li, M.; Liu, J. *J. Phys. Chem. C* **2009**, *113*, 9581−9587.
(14) Huang, J.; Matsunaga, N.; Shimanoe, K.; Yamazoe, N.; Kunitake, T. *Chem. Mater.* **2005**, *17*, 3513−3518.
(15) Song, X.; Gao, L.; Mathur, S. *J. Phys. Chem. C* **2011**, *115*, 21730−21735.
(16) Chen, J.; Xu, L.; Li, W.; Gou, X. *Adv. Mater.* **2005**, *17*, 582−586.
(17) Kim, W.-S.; Lee, B.-S.; Kim, D.-H.; Kim, H.-C.; Yu, W.-R.; Hong, S.-H. *Nanotechnology* **2010**, *21*, 245605.
(18) Vayssieres, L.; Keis, K.; Hagfeldt, A.; Lindquist, S.-E. *Chem. Mater.* **2001**, *13*, 4395−4398.
(19) Wang, H.; Li, G.; Jia, L.; Wang, G.; Tang, C. *J. Phys. Chem. C* **2008**, *112*, 11738−11743.
(20) Elias, J.; Tena-Zaera, R.; Wang, G.-Y.; Lévy-Clément, C. *Chem. Mater.* **2008**, *20*, 6633−6637.
(21) Li, Q.; Kumar, V.; Li, Y.; Zhang, H.; Marks, T. J.; Chang, R. P. *Chem. Mater.* **2005**, *17*, 1001−1006.
(22) Yu, H.; Zhang, Z.; Han, M.; Hao, X.; Zhu, F. *J. Am. Chem. Soc.* **2005**, *127*, 2378−2379.
(23) Jia, C. J.; Sun, L. D.; Yan, Z. G.; You, L. P.; Luo, F.; Han, X. D.; Pang, Y. C.; Zhang, Z.; Yan, C. H. *Angew. Chem.* **2005**, *117*, 4402−4407.
(24) Liu, J.; Li, Y.; Fan, H.; Zhu, Z.; Jiang, J.; Ding, R.; Hu, Y.; Huang, X. *Chem. Mater.* **2009**, *22*, 212−217.
(25) Zhang, J.; Liu, X.; Zhang, L.; Cao, B.; Wu, S. *Macromol. Rapid Commun.* **2013**, *34*, 528−532.
(26) Wang, X.; Li, Y. *Chem.—Eur. J.* **2003**, *9*, 5627−5635.
(27) Zhang, J.; Wang, S. R.; Xu, M. J.; Wang, Y.; Zhu, B. L.; Zhang, S. M.; Huang, W. P.; Wu, S. H. *Cryst. Growth Des.* **2009**, *9*, 3532−3537.
(28) Liu, X. H.; Zhang, J.; Wang, L. W.; Yang, T. L.; Guo, X. Z.; Wu, S. H.; Wang, S. R. *J. Mater. Chem.* **2011**, *21*, 349−356.
(29) Zhang, J.; Wang, S. R.; Wang, Y.; Xu, M. J.; Xia, H. J.; Zhang, S. M.; Huang, W. P.; Guo, X. Z.; Wu, S. H. *Sens. Actuators, B* **2009**, *139*, 369−374.
(30) Chiu, H.-C.; Yeh, C.-S. *J. Phys. Chem. C* **2007**, *111*, 7256−7259.
(31) Barsan, N.; Koziej, D.; Weimar, U. *Sens. Actuators, B* **2007**, *121*, 18−35.
(32) Jinkawa, T.; Sakai, G.; Tamaki, J.; Miura, N.; Yamazoe, N. *J. Mol. Catal. A: Chem.* **2000**, *155*, 193−200.
(33) Kuang, Q.; Lao, C. S.; Wang, Z. L.; Xie, Z. X.; Zheng, L. S. *J. Am. Chem. Soc.* **2007**, *129*, 6070−6071.
(34) Barsan, N.; Weimar, U. *J. Phys.: Condens. Matter* **2003**, *15*, R813−R840.
(35) Yamazoe, N.; Shimizu, Y. *Sens. Actuators, B* **1986**, *10*, 379−398.